A search for thermal excursions from ancient extraterrestrial impacts using Hadean zircon Ti-U-Th-Pb depth profiles

Sunshine S. Abbott[a], T. Mark Harrison[a,1], Axel K. Schmitt[a], and Stephen J. Mojzsis[b,c]

[a]Department of Earth and Space Sciences, University of California, Los Angeles, CA 90095; [b]Department of Geological Sciences, University of Colorado, Boulder, CO 80309; and [c]Laboratoire de Géologie de Lyon, Ecole Normale Supérieure de Lyon and Université Claude Bernard Lyon 1, 69007 Lyon, France

Few terrestrial localities preserve more than a trace lithic record prior to *ca.* 3.8 Ga greatly limiting our understanding of the first 700 Ma of Earth history, a period inferred to have included a spike in the bolide flux to the inner solar system at *ca.* 3.85–3.95 Ga (the Late Heavy Bombardment, LHB). An accessible record of this era may be found in Hadean detrital zircons from the Jack Hills, Western Australia, in the form of μm-scale epitaxial overgrowths. By comparing crystallization temperatures of pre-3.8 Ga zircon overgrowths to the archive of zircon temperature spectra, it should, in principle, be possible to identify a distinctive impact signature. We have developed Ti-U-Th-Pb ion microprobe depth profiling to obtain age and temperature information within these zircon overgrowths and undertaken a feasibility study of its possible use in identifying impact events. Of eight grains profiled in this fashion, four have overgrowths of LHB-era age. Age vs. temperature profiles reveal a period between *ca.* 3.85–3.95 Ga (i.e., LHB era) characterized by significantly higher temperatures (approximately 840–875 °C) than do older or younger zircons or zircon domains (approximately 630–750 °C). However, temperatures approaching 900 °C can result in Pb isotopic exchange rendering interpretation of these profiles nonunique. Coupled age-temperature depth profiling shows promise in this role, and the preliminary data we report could represent the first terrestrial evidence for impact-related heating during the LHB.

early Earth | impact crater | lunar cataclysm | secondary ion mass spectrometry

The LHB is the period from *ca.* 3.85–3.95 Ga during which an intense flux of asteroidal and/or cometary bodies is hypothesized to have impacted the Moon (1). A variety of theories have been proposed to explain the LHB (2–5) culminating with the "Nice model" (5–7). This model posits that a fundamental shift in orbital resonance among the Jovian planets at *ca.* 3.9 Ga destabilized the disk of planetesimals in the outer solar system resulting in the scattering of numerous bodies into the inner solar system.

Tera et al. (1) introduced the concept of a late lunar cataclysm to explain isotopic fractionations in rocks returned from the heavily cratered lunar highlands. Specifically, U-Pb, and Rb-Sr isochrons yielded recrystallization ages between 3.85–3.95 Ga. The parent/daughter behavior in these two geochronologic systems are quite different but result in similar system disturbances (i.e., U and Sr are highly refractory whereas Pb and Rb are variably volatile). Thus, a profound thermal event, such as from an impact at the appropriate scale of a "cataclysm," could have caused resetting of both chronometers, albeit for different reasons. Much of the evidence in support of the LHB hypothesis comes from $^{40}Ar/^{39}Ar$ age spectra of lunar highland crust samples (3, 8, 9), interpreted to yield apparent "plateau" ages between 3.8–4.0 Ga due to the resetting of the K-Ar system via collisional heating (see review in 10). This hypothesis, however, remains controversial (e.g., refs. 11–14).

Whereas an early impact record is preserved on the lunar surface and in some meteorites, the terrestrial rock record prior to approximately 3.8 Ga is scant thus severely limiting the search for evidence of the LHB on Earth (cf. 15). A potential source of such evidence is from Hadean (i.e., >4 Ga) detrital zircons (16). Because zircon is essentially restricted to the Earth's crust and Archean continental crust is thought to have been relatively thin due to high heat flow (e.g., 17), the vast majority of Hadean zircons of continental character likely resided within *ca.* 30 km of the Earth's surface during the LHB. This proximity to the surface permits ancient zircons to have recorded thermal signatures of large impacts on the early Earth. It is well established that zircons are excellent geochronometers due to their initial enrichments in U and Th parent isotopes relative to daughter Pb* and their resistance to alteration by weathering, dissolution, shock, and diffusive exchange (18–24). Although zircons investigated in this study are detrital (i.e., they have been removed from their original petrologic context), their isotopic signatures can provide substantial information regarding the continuum of environmental conditions they experienced owing to their durability and tendency to form epitaxial overgrowths during thermal metamorphism (20).

We obtained time-temperature profiles with depth in zircons by combining empirical Ti-in-zircon thermometry (25, 26) with ultrahigh resolution (nm scale) U-Th-Pb depth profiling (16, 27). The ultimate goal is to obtain sufficient data to reconstruct a T-t path for each zircon's growth and compare results with LHB thermal models (28).

Experimental Procedures

Hadean Zircon Samples. Hadean zircons have been identified from multiple regions around the globe including northern Canada (29), West Greenland (30), and Western Australia (31). However, the most extensively studied are those from the Narryer Gneiss Complex (NGC), located on the northern margin of the Yilgarn Craton, Western Australia (32–35). First recognized at outcrops near the Mt. Narryer homestead (31), even more ancient Hadean zircons were documented in the Jack Hills region (36).

The Jack Hills constitute a narrow and sheared supracrustal belt (*SI Appendix*, Fig. S1) (37) with a diverse assemblage of metasedimentary rocks that appear to have been deposited at *ca.* 3.1 Ga (31, 36). Detrital zircons with $^{207}Pb/^{206}Pb$ ages in excess of approximately 4 Ga predate the LHB era but comprise only a few percent of zircons within the metasedimentary rocks (38, 39). In the Jack Hills, most detrital zircons range in age from 3.7–3.1 Ga (40) with some <3.1 Ga (41), likely due to radiogenic

Pb loss. Approximately 3% of Jack Hills zircons are between 4.3 and 3.9 Ga with only 0.04% $\geq$ 4.3 Ga (39, 41–44). We utilized the archive of Hadean Jack Hills zircons U-Pb age characterized via conventional ion microprobe spot analysis (i.e., a three cycle analysis) in the study of Holden et al. at Australian National University (ANU) (39). Selected grains have $\geq$95% U-Pb concordant primary core crystallization ages between 4.0–4.1 Ga thus predating the inferred LHB era.

Zircon Standards. Duluth Complex anorthositic series (AS3) zircon served as the primary geochronological reference standard (1099 $\pm$ 1 Ma) (45, 46). U and Th concentrations were obtained by comparing $^{238}U^+/^{94}Zr_2{}^{16}O^+$ and $^{232}Th^+/^{94}Zr_2{}^{16}O^+$ ratios in the unknown grains with those in megacryst zircon standard 91500 (U = 81.2 ppm; Th/U = 0.3) (47). AS3 zircon (48), by contrast, shows highly variable U and Th abundances here and other studies (49) and is thus not suited as a U and Th concentration standard. We determined the concentration of Ti by directly comparing $^{49}Ti^+/^{94}Zr_2{}^{16}O^+$ between AS3 and the unknown assuming an AS3 [Ti] of 5.25 ppm (50).

U-Th-Pb Depth Profiling. The U-Th-Pb depth profiling technique permits age variations to be measured in the near-surface region of crystals at the highest possible spatial resolution (51). An optical profilometer is used to measure the depth of analysis pits in zircon standards and, thus, translate analysis time into depth. In this fashion, we have been able to reproducibly assess when sputter pits are *ca.* 5 μm deep, at which point the secondary ion extraction geometry changes causing a breakdown of the interelement (e.g., Pb/U) calibration.

Zircon Titanium Thermometry (T^{xlln}). The Ti content of zircon has been shown to behave as a crystallization thermometer (25, 52) as its concentration is a simple function of temperature if the activity of rutile (a_{TiO_2}) is buffered at a constant value. Ferry and Watson (2007) (26) subsequently revised the calibration to include the influence of a_{TiO_2} and a_{SiO_2} Ti solubility in zircon. The dependency of the thermometer on pressure is relatively low for zircon formed below approximately 10 kbar such that an uncertainty of $\pm$10 kbar induces an uncertainty of 50 °C at 750 °C (26). Although detrital zircons may have unconstrained a_{TiO_2} and a_{SiO_2} (unless quartz and rutile inclusions are present), most igneous and metamorphic rocks have a_{TiO_2}, and $a_{SiO_2} \geq 0.5$ (25, 26).

Ti-U-Th-Pb Depth Profiling. Extension of depth profiling to combine U-Th-Pb geochronology and T^{xlln} permits revealing age and temperature profiles at sub-μm resolution. This new capability holds the potential to identify when and under what thermal conditions small overgrowths in minerals such as zircon formed. Despite the substantial range between the masses of interest (i.e., $^{238}U^{16}O$ to ^{49}Ti) and the potential for significant hysteresis during magnet switching, we found that peak-hopping between mass 49–254 to attain flat-topped peaks at a mass resolving power (MRP) of *ca.* 4,500 required only a *ca.* 10 s settling time.

Analytical procedures for depth profiling zircons were broadly similar to those outlined in Grove and Harrison (51). Because of the tabular geometry typical of zircon and the generally symmetric nature of overgrowths, we were able to use large primary beam diameters (e.g., 30–50 μm) to enhance signal strength. We centered the secondary ion image within a small contrast diaphragm and field aperture prior to each analysis to better restrict transmission to ions originating from the crater bottom. A 15–20 nA O$^-$ primary beam current was used with an approximately 10 kV secondary beam accelerating voltage. We assessed the appropriate energy offset for the various species of interest (i.e., different elements have differing secondary ion energy spectra) by scanning the secondary acceleration voltage on standard zircons and maintained a stable energy distribution region for analysis

of U, Pb, and UO via automated rescanning during each depth profile. Each depth profile analysis session began with depth profiling a 91500 zircon in order to calibrate the elemental abundances, followed by an AS3 depth profile to calibrate the U/Pb sensitivity in each unknown grain. Data reduction for zircons was performed using in-house software package ZIPS v3.04. We used Stacey and Kramers' (53) Pb evolution model to correct for common Pb (*SI Appendix*, Figs. S2 and S3).

Results

Ti-U-Th-Pb Depth Profiles. Ti-U-Th-Pb depth profile segments of zircons are categorized in order as P1, P2, P3, and P4. Three analyses cycles (i.e., a full cycle through the analyzed peaks) in the depth profiles were averaged together into one "block" to enhance precision by improving counting statistics. The samples are from the Research School of Earth Sciences (RSES) collection at ANU. Thus RSES61-2.6 represents the zircon in row two, column six in mount RSES61. Hereafter, the grains analyzed are referred to simply by their numerical designation. The zircons have 98–100% radiogenic ^{206}Pb except where otherwise stated.

An approximately 9.4 μm depth profile obtained on 61–2.6 reveals an isochronous distribution of $^{207}Pb/^{206}Pb$ ages with an average of 3,997 $\pm$ 15 Ma to 6.2 μm (*SI Appendix*, Fig. S4). Th/U ratios remain 0.3 throughout the profile and [U] ranges between 173 ppm and 246 ppm. The implausibly old (4,524 $\pm$ 322 Ma to 5,091 $\pm$ 331 Ma) and reversely concordant $^{206}Pb/^{238}U$ ages from P1 may be due to unrecognized interelement calibration errors. P2 reveals age scatter between 4,053 $\pm$ 11 Ma and 4,087 $\pm$ 20 Ma (older than the core age), which may indicate zircon orientation complexities when previously obtaining the core age. Oscillation in [U] from 258 ppm to 292 ppm is shown over P2, and U-Pb concordance is relatively high at *ca.* 95%. Calculated crystallization temperatures decrease from 682 °C to 635 °C over P1 and increase from 646 °C to 662 °C over P2.

Grain 61-4.9 was analyzed along an approximately 28 μm depth profile. $^{207}Pb/^{206}Pb$ ages decrease within 1 μm and subsequently increase to 4,020 $\pm$ 8 Ma to a depth of 17.2 μm (*SI Appendix*, Fig. S6). Near-surface ages have high errors as a result of high ^{204}Pb as shown by low radiogenic yields. Extremely low U-Pb concordance values (e.g., 3%) from P1 correspond to relatively high [U] values (e.g., 11,000 ppm). Th/U ratios are initially *ca.* 3.0 and decrease to 1.1 by 11.6 μm. U-Pb concordance increases from 28% to 77%, whereas [U] decreases from 252 ppm to 164 ppm over P2. $^{207}Pb/^{206}Pb$ ages fluctuate between 4,012 $\pm$ 63 Ma and 4,044 $\pm$ 33 Ma and Th/U values decrease from 2.0 to 1.7 over P3. Low concordance shown from P3 (e.g., 26%), corresponds with a [U] decrease from 538 ppm to 392 ppm. Beyond 23 μm, near-core ages are revealed. After 13.2 μm, Th/U values oscillate and subsequently increase to 0.7. U-Pb concordance and [U] fluctuates over P4 between 49–77% and 83–209 ppm, respectively. Initial calculated temperatures from P1 (e.g., 2005 °C) are clearly fictive (i.e., zircon breaks down to ZrO_2 and SiO_2 at approximately 1,660 °C), thus these apparent high temperatures may be artifacts of contamination. Temperatures decrease to 1,045 °C by the end of P1. Temperature further declines over P2 from 870 °C to 795 °C, whereas P3 reveals a higher initial temperature of 971 °C and peaks at 1,094 °C by 19.8 μm. P4 reveals a semicontinuous decrease in temperature from 1,087 °C to 732 °C.

Zircon 61-8.2 was depth-profiled to approximately 8.6 μm. An isochronous distribution of near-core $^{207}Pb/^{206}Pb$ ages is revealed over 4.7 μm. Subsequent ages fluctuate between 3,884 $\pm$ 13 Ma and 3,975 $\pm$ 22 Ma (*SI Appendix*, Fig. S8). Th/U ratios exhibit a decrease from 1.9 to 0.9 by 5.4 μm. Th/U decreases from 1.6 to 1.1 followed by an increase to 1.3 by 8.6 μm. U-Pb concordance increases from 28% to 65% over P1 and fluctuates to a final value of 62% over P2. P1 reveals a decrease in temperatures from 1,053 °C to *ca.* 900 °C. Calculated temperatures from P2 decrease from 923 °C to 875 °C.

An approximately 16.5 μm depth profile was attained on 68-1.1. P1 reveals a ^{207}Pb/^{206}Pb age gradient from $3,259 \pm 25$ Ma to $3,422 \pm 19$ Ma followed by a sharper increase to $3,667 \pm 36$ Ma by 8.6 μm (*SI Appendix*, Fig. S10). Ages from P2 increase from $3,837 \pm 20$ Ma to $4,117 \pm 10$ Ma. [U] initially decreases from 974 ppm to 265 ppm and afterwards shows a parabolic trend before fluctuating at values <200 ppm beyond 7 μm in depth. Th/U ratios oscillate between 1.4 and 0.2–8.2 μm and subsequently level out at *ca.* 0.4. Degree of U-Pb concordance increases from 41% to 98% by 6.0 μm and is reversely concordant thereafter (i.e., U-Pb concordance ranges between 102–123%). P1 yields temperatures decreasing from 1,405 °C to 1,066 °C. Subsequent temperatures vacillate between 682 °C and 868 °C before leveling out at *ca.* 700 °C by 12.0 μm. The AS3 profiled prior to this zircon shows a homogeneous temperature distribution; therefore, the variation in temperatures calculated for 68–1.1 is unlikely to result from analytical artifacts (*SI Appendix*, Fig. S11).

An approximately 17 μm depth profile was conducted on 68-3.7. ^{207}Pb/^{206}Pb ages from P1 reveal a fluctuating distribution between $3,994 \pm 25$ Ma and $4,040 \pm 4$ Ma (*SI Appendix*, Fig. S12). P2 ages oscillate from $3,983 \pm 23$ Ma to $4,089 \pm 4$ Ma. Variations in ages may be explained by analytical procedure because the AS3 analyzed prior to P1 (*SI Appendix*, Fig. S13) shows similar trends (i.e., ages vary between $1,048 \pm 23$ Ma and $1,130 \pm 22$ Ma). Th/U ratios remain 0.4 throughout the profiles. P1 yields reversely concordant values (i.e., >100%) due to absurdly high ^{206}Pb/^{238}U ages and errors ranging from $4,279 \pm 249$ Ma to $4,809 \pm 361$ Ma. Ages from P2 are nearly 100% or >100% concordant. [U] from P1 and P2 oscillates from 169 ppm to 237 ppm and from 194 ppm to 235 ppm, respectively. P1 reveals temperatures fluctuating between 693 °C and 715 °C; whereas, P2 provided slightly higher temperatures ranging from 713 °C to 729 °C.

A *ca.* 8.5 μm depth profile indicates a ^{207}Pb/^{206}Pb age distribution similar to the core age of 68-19.9 (*SI Appendix*, Fig. S14); therefore, this grain was not considered for further analysis. The average age is $4,027 \pm 28$ Ma (Mean Square Weighted Deviation, MSWD = 0.65). The Th/U values are *ca.* 0.4. Degree of U-Pb concordance varies from 95% up to reversely concordant values. [U] decreases semicontinuously from 90 ppm to 37 ppm and subsequently increases to 101 ppm. Calculated temperatures fluctuate from 668 °C to 690 °C.

Grain 71-3.4 was analyzed along an approximately 17 μm depth profile. Ages from P1 (*SI Appendix*, Fig. S16) yield a slightly fluctuating distribution from $3,982 \pm 9$ Ma to $4,028 \pm 4$ Ma, with an average of $4,006 \pm 14$ Ma (MSWD = 3.2). P2 provides a similar dispersion ranging from $3,986 \pm 10$ Ma to $4,037 \pm 7$ Ma and an average age of $4,009 \pm 18$ Ma (MSWD = 2.6). The Th/U ratios remain *ca.* 1.9. The first nine ages are <100% concordant and values thereafter are >100% to 17 μm. P1 and P2 reveal fluctuating [U] ranging from 195–288 ppm and 186–254 ppm, respectively. P1 yields temperatures between 718 °C and 736 °C with the exception of one 685 °C outlier. P2 yields temperatures ranging from 718 °C to 740 °C.

A 25.5 μm depth profile was conducted on zircon 71-7.2. ^{207}Pb/^{206}Pb ages increase from $3,640 \pm 46$ Ma to $3,933 \pm 36$ Ma over P1 and from $3,943 \pm 28$ Ma to $3,992 \pm 46$ Ma over P2 (Fig. 1*A*). Ages from P3 vary from $3,941 \pm 40$ Ma to $4,027 \pm 11$ Ma. [U] decreases from 664 to 186 ppm over P1 (Fig. 1*B*). P2 and P3 reveal [U] oscillating between 127 and 189 ppm and from 125 to 173 ppm, respectively. Th/U ratios decrease from 3.9 to 2.3 and afterwards semi-continuously increase to ~3.0 to 8.5 μm. Th/U values decrease from 2.4 to 1.3 over P2 and from 0.8 to 0.6 over P3. U-Pb concordance from P1 and P2 increases from 32–60% and 71–87%, respectively (Fig. 1*C*). Degree of concordance from P3 decreases from 79–63% and subsequently increases to 90%. ^{206}Pb/^{238}U ages from P1 increase from 94 to 98% radiogenic. Temperatures decrease from 1,102 °C to 844 °C by 8.5 μm. Calcu-

Fig. 1. Ti-U-Th-Pb depth profiled zircon 71-7.2.

lated temperatures from P2 and P3 decrease from 844 °C to 788 °C and 774 °C to 755 °C, respectively.

^{57}Fe Analysis. The isotope ^{57}Fe was included in the run table for depth profiling as Fe has been inferred to act as a monitor of external contamination. The ^{57}Fe/^{94}Zr$_2$O ratios from AS3 grains are used as a proxy for contamination in the Hadean zircons, which generally decrease at the onset of depth profiles, indicating possible contamination to a depth of approximately 1 μm. The 71-3.4 AS3 grain has relatively high initial ^{57}Fe/^{94}Zr$_2$O ratios (e.g., 5.2). AS3 zircons analyzed prior to 71-7.2 and 61-2.6 have ratios that increase from 0.005 to 0.03 and decrease from 0.89 to 0.007, respectively. The 68-19.9 AS3 yields *ca.* 0.001 ratios. AS3 zircons' ^{57}Fe analyzed in conjunction with 61-4.9, 61-8.2, and 68-3.7 decrease by an order of magnitude (e.g., the 61-4.9 AS3 ratios decrease from 0.07 to 0.004) to approximately 1 μm and thereafter remain constant. Thus, we have labeled data that may be an artifact of contamination as open red hexagons on the T^{xlln} plots (*SI Appendix*, Figs. S4A–S18A and Fig. 1).

Discussion

Overview. While the rare terrestrial lithic record prior to >4 Ga limits the search for evidence of the LHB on Earth, Hadean detrital zircons may provide a source of such evidence (16). Zircon chemistry may be used to derive temperatures that provide insight into environmental source conditions during crystal growth. A significant question to ask is: Are any LHB-era thermal

excursions preserved in zircon indicative of growth during impact heating? An answer may be ascertained by evaluating whether Hadean zircon LHB-era overgrowths formed under such anomalously high temperatures that we are persuaded to interpret their growth as a response to impact heating during the LHB. This can be done by comparing crystallization temperatures of LHB-era zircons to temperature spectra of terrestrial Hadean zircons and impact-formed zircons. Jack Hills zircons with ages between *ca.* 3.4–3.85 Ga reveal an average crystallization temperature of 679 ± 124 °C (54). Terrestrial Hadean zircons yield temperatures ranging from 600–780 °C with a tight cluster at 680 ± 25 °C (25, 55); whereas, zircons formed during large terrestrial impact events ranging from the Archean to Phanerozoic yield a much higher average temperature of 770 °C (56). Discriminating actual overgrowths from near surface regions that have experienced diffusion loss of Pb* is not unambiguous. In certain cases, corresponding changes in age and trace element chemistry may be evidence for the former, and the very slow rate of Pb transport under crustal conditions limits the extent of diffusion exchange (57). We assume that age contrasts reflect episodic or continuous growth unless diffusion exchange can be unambiguously established. For example, a constant Ti-derived temperature across a zone of varying age is interpreted as an overgrowth. Interpreting some ages as overgrowths that correspond to repolishing interfaces is problematic as some material may have been removed during the polishing steps. Several results, however, yield uniform $^{207}Pb/^{206}Pb$ ages we interpret as epitaxial zircon overgrowths. We observed evidence of scouring of crater bottoms after repolishing using 1 and ¼ μm diamond polish. We attempted to remediate this problem by polishing instead with Fibromet SiC paper such that the vestigial pit was at least 1–2 μm deep in an attempt to preserve pit visibility and integrity. Even in this case, minor age and concentration discontinuities were seen. The effect of other analytical artifacts including noncoincident centering of the primary beam following polishing, nonplanar initial surfaces, varying sample sputter efficiency, and nonuniformity of primary beam intensity (even with Kohler illumination) are difficult to assess but collectively would lead to the blurring of sharp discontinuities.

Four of the eight zircons Ti-U-Th-Pb depth profiled have LHB-era overgrowths. 61-4.9 and 71-7.2 reveal overgrowths that formed by continuous slow growth. 68-1.1 reveals an age gap between approximately 3,670–3,830 Ma; however, a subsequent LHB-era overgrowth shows continuous growth starting at 3,830 Ma. Although 61-8.2 appears to have been initially profiled over the core, successive $^{207}Pb/^{206}Pb$ ages reveal an overgrowth *ca.* 3,900 Ma. Whereas the four remaining zircons profiled have $^{207}Pb/^{206}Pb$ ages *ca.* 3,950 Ma, the majority of ages are at or near the core age of these grains. All Ti-U-Th-Pb depth profiles of 61-2.6, 68-3.7, 68-19.9, and 71-3.4, along with the last depth profile for 68-1.1, cluster strongly with ages >3980 Ma and temperatures between 630–750 °C. The last depth profile of 71-7.2 yields ages ranging from 3,940–4,030 Ma and temperatures from approximately 750–780 °C. Grain 61-4.9 reveals ages >3,990 Ma showing a diminution in crystallization temperatures over the final profile from 955 °C down to 732 °C. Thus, seven of the eight zircons provide $^{207}Pb/^{206}Pb$ ages >3,940 Ma with temperatures ranging from approximately 630–780 °C, which is consistent with crystallization temperatures of terrestrial Hadean zircons (e.g., 600–780 °C).

Four grains reveal age domains clustering between 3,800 Ma and 4,000 Ma and temperatures between 780 °C and 900 °C. P2 and P3 of 71-7.2 as well as P2 of 61-8.2 yield temperatures between approximately 780–900 °C. Ages from P2 of 61-4.9 are >3,830 Ma and temperatures range from 800–885 °C. While 68-1.1 reveals LHB-era ages with temperatures overlapping terrestrial Hadean zircon crystallization temperatures that range from 600 °C and 780 °C (25, 55), the majority of LHB-era temperatures are between 780 °C and 900 °C, which is consis-

tent with impact temperature spectra ranging from 680 °C to 900 °C (56).

Virtually all depth profile analyses reveal discordant U-Pb ages. This discrepancy indicates pervasive Pb-loss within the subsurface regions of the Hadean zircons following primary core crystallization or artifacts of the Pb/U relative sensitivity calibration. While Pb-loss and U-Pb discordance can be a result of diffusion or leaching, these mechanisms do not account for the apparent enrichment in U, Th, and Pb. U-Pb ages from 3,950 Ma to 4,100 Ma are between 80–130% concordant. Reversely concordant values up to 180% are obtained for some U-Pb ages between 3,350 Ma and 4,180 Ma with a tight cluster from 100–130% for U-Pb ages between 3,900 Ma and 4,100 Ma. Whereas some U-Pb ages are concordant near the core, the vast majority are reversely concordant, thus U-Pb ages are viewed as suspect and provide reasoning to report $^{207}Pb/^{206}Pb$ ages rather than U-Pb ages for these ancient zircons. An extensive follow-up study would be necessary to gain a comprehensive understanding regarding U-Pb concordance complexities with depth in zircon.

We examined the relationship between Fe and Ti in the depth profiles and found both higher Fe levels in the unknowns relative to the standards and correlations between Fe and Ti in the unknowns. In cases where exceedingly high Ti concentrations imply improbably high temperatures, this must represent ingress of contaminating Fe, probably along cracks. However, the coherent nature of Ti profiles such as Fig. 1 and systematic relationships (e.g., anticorrelations between U and Ti) appear inconsistent with such a mechanism. We note that the ionic radius of Fe^{3+} in VIII-fold coordination (0.78) is close to that for VIII-fold Zr^{+4} (0.84) (58), and, thus, Fe^{3+} may dissolve in zircon at relatively high levels under the high Fe_2O_3 activity expected for oxidizing crustal conditions. However, we caution that even apparently coherent Ti profiles could reflect contamination.

Correlated Age/Temperature Analysis. The Probability Density Function (PDF) is the summation of individual Gaussian distributions for each datum in a population. Thus, the probability distribution for an individual parameter such as $^{207}Pb/^{206}Pb$ age can be obtained for information content analysis via describing the size or "density" distribution of said parameter. The Cumulative Distribution Function (CDF) is the probability that a random variable, x, with a specific PDF will be found at a value less than or equal to x. However, for us to resolve variations in thermal conditions as a function of age, a statistical method that accounts for errors in both parameters would best reveal possible correlations. In such cases, we use a 2D PDF. Data were "smoothed" by assigning a Gaussian uncertainty distribution of 1σ for the measurements.

1D Probability Density Functions. Assessing the temperature-age relationships among LHB-era zircons requires an extensive sampling of the overgrowths within the detrital population. For additional details regarding LHB-era zircon overgrowths identified via U-Th-Pb depth profiles, refer to Trail et al. (16) and Abbott (59). A PDF and CDF are graphically represented for $^{207}Pb/^{206}Pb$ age (Fig. 2 A and B) and temperature (Figs. 2 C, D and 3) for the Ti-U-Th-Pb depth profiled zircons. The highest density of ages is at 4,000 Ma, and the probability of an age being ≥4, 000 Ma is 54%. There is an approximately 15% probability of obtaining an LHB-era age within a random selection of the total ages. The highest density peak of temperatures is at 714 °C. There is an approximately 80% probability that a randomly selected temperature will fall between 630 °C and 900 °C. Approximately 9% of the temperatures are relatively very high (i.e., 1,100 °C–2,005 °C), which are likely artifacts of contamination and, thus, are omitted from the probability plots. There is an approximately 34% probability of obtaining a temperature between 680–740 °C, and an approximately 52% probability that a temperature will fall above 740 °C. Temperatures between 640 °C and 680 °C are
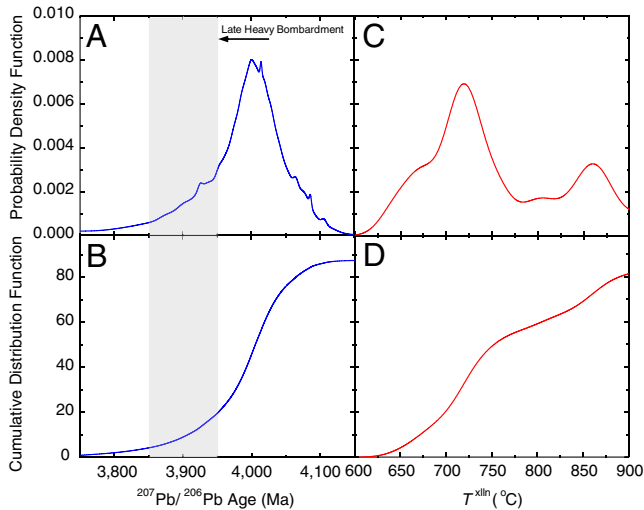
Fig. 2. 1D probability density function and cumulative distribution function plots.

calculated for 14% of the zircons. Many crystallization temperatures from the Ti-U-Th-Pb depth profiles are consistent with impact produced zircon temperatures (Fig. 3).

2D Probability Density Functions. The 2D probability density function allows us to determine temperature variations as a function of age. Blue represents the least probable density level and subsequent colors show the probability density levels separated by a factor of approximately 1.0; however, within an individual color the increasing color gradient represents a slight density accession (Fig. 4). There are generally two broad clusters with calculated ages of ≥3,940 Ma with temperatures between 630–780 °C, and ages ranging from *ca.* 3,800–3,940 Ma with corresponding temperatures between 780–900 °C. The probability of determining a temperature of 726 °C at an age of 4,013 Ma is highest at 50% [shown in red (Fig. 4)]. There is a relatively high density cluster (shown in yellow) with ages between 3,990 Ma and 4,020 Ma and temperatures from 715 °C to 730 °C. Approximately 11% of data from these zircons reveal temperatures from 900 °C to 1,100 °C within ages between 3,940 Ma and 4,040 Ma and, for scaling purposes, were omitted from this plot (i.e., due to the very large temperature range from the likelihood of contamination, data >900 °C were not clearly expressed).
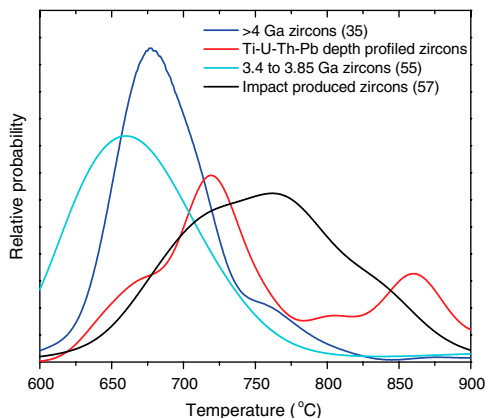
A large number (approximately 48%) of ages >4,000 Ma fall between relatively low temperatures of 670 °C and 740 °C. Ages ranging from 3,950 Ma to 4,000 Ma have a broad range of temperatures between 630 °C and 870 °C and represent approximately 28% of the data. The probability of determining an age between 3,900–3,950 Ma with temperatures from 840 °C to 880 °C is 10%. There is a 5% probability of obtaining an age between 3,850 Ma and 3,900 Ma with a temperature between 850–875 °C. An approximately 3% probability exists for determining an age ranging from 3,800 Ma to 3,850 Ma with a temperature in between 860 °C and 865 °C. Inspection of the frequency distribution shows that the temperatures in between ages of 3,800 Ma and 4,000 Ma are broadly between 630 °C and 875 °C; however, the lower ages (*ca.* 3,900 Ma) generally have higher temperatures (*ca.* 860 °C). We emphasize that, due to the unknown rutile activity during zircon growth, these temperatures may be underestimated by >50 °C (25).

Zircon overgrowths can grow under metamorphic and igneous conditions. Our geochemical studies are insufficient to select between these two environments but both are likely processes associated with impacts. For example, Abramov and Mojzsis (28) calculated that the LHB bombardment episode would have resurfaced about a quarter of the Earth. Wielicki et al. (56) developed a model to assess the temperature distribution of zircons grown from impact melts during a bombardment episode of the inferred scale of the LHB. They estimated that 37% of the crust would be processed through impacts during an LHB-type event with about 6% overlap (i.e., approximately 1/3 of the crust). From these zeroth-order estimates, we can reasonably infer that approximately one quarter to half of the crust would have potentially experienced conditions conducive to zircon reprocessing/growth. Thus our observation that 12 of the 26 Hadean zircons thus far investigated via depth profiling (including 18 U-Th-Pb depth profiles) (16, 59) experienced epitaxial growth between 3.85–3.95 Ga is consistent with this estimate. However, our empirical observations do not include the possibility that overgrowths grown during the LHB-era on Hadean cores may have been abraded prior to deposition in the host quartzite at *ca.* 3.1 Ga and, thus, would provide a lower bound.

Detailed Profile Interpretations. While the identification of broad age vs. temperature trends (Fig. 4) is encouraging, it omits a key advantage of our method—the documentation of continuous temperature-time profiles. That is, interpretations drawn from the age-temperature PDF must be consistent with thermal histories derived from individual overgrowths. One caveat is to note that apparent age (and trace element) gradients can arise from discontinuous boundaries if the overgrowth/core interface is not
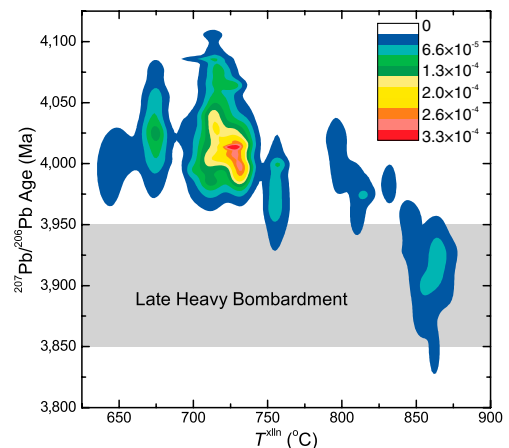

Fig. 3. 1D relative probability vs. T^{xlln} plot of Hadean zircons (35, 55, 60) and melt sheet impact produced zircons (57). The highest peak of temperatures from this study range between approximately 680–750 °C. The offset of their maxima to higher temperatures indicates a bimodal temperature distribution.

Fig. 4. 2D $^{207}Pb/^{206}Pb$ age and T^{xlln} relative probability plot. The shaded region indicates the LHB-era. The seven colors shown are, from the top to the bottom in the key, of increasing constant probability density.

perpendicular to the surface of the epoxy mount (or if the interface is not planar). Thus, for example, the 3.0–3.8 Ga gradient seen in profile 61-4.9 between 2–8 μm depth could potentially represent a sharp interface between 3 Ga and 3.8 Ga domains that has been blurred by nonnormal penetration of the core. However, abrupt discontinuities in simultaneously measured trace elements, such as the variations in Ti seen between 4–6 μm depth, are evidence that the depth resolution is at a much finer scale than that of the age gradient.

Profiles for grains 61-2.6, 68-3.7, 68-19.9, and 71-3.4 generally reveal age vs. temperature histories that are typical of that seen in Hadean detrital zircons (>4 Ga, 750–650 °C) (35) and, thus, will not be discussed further.

Several aspects of the 61-4.9 profile are worth noting (*SI Appendix*, Fig. S6). Temperatures vary from 700 to >1,400 °C and [U] rises to >1,000 ppm. Portions with [U] >200 ppm correspond to <50% concordance (i.e., due to radiation damage) and low radiogenic yields. While we are reluctant to derive detailed thermal history information from across this overgrowth, we remain confident that the age vs. temperature data from the low (<200 ppm) [U] regions is meaningful.

Overgrowth 61-8.2 presents a special case in that age appears to decrease with increasing depth along the profile (*SI Appendix*, Fig. S8). Clearly this is a paradox; the latest grown portion cannot be older than an earlier overgrowth. However, the anomalously old portion is associated with high [U] (400–1,000 ppm) and low (<60%) concordance. High [U] zircons are susceptible to U loss (60) that moves the age along a trajectory on concordia opposite to Pb loss. Any subsequent Pb loss results in apparent $^{207}Pb/^{206}Pb$ ages that are older than the true age (61). Detailed interpretation of this profile appears unwarranted.

Profile 68-1.1 shows relatively low U-Pb concordance (e.g., 80%) associated with >300 ppm [U] (*SI Appendix*, Fig. S10). A parabolic trend in [U] corresponds to nearly 100% concordance along with a similar trend in temperatures ranging from *ca.* 650 to 875 °C. The deepest portion of this profile records temperatures similar to that of Hadean terrestrial zircons (*ca.* 650–775 °C). Because the diffusivity of Pb is so low as to make it immobile over geological durations, this age-temperature profile can be directly interpreted from (*SI Appendix*, Fig. S10).

Profile 71-7.2 shows three broad cycles of decreasing U with the second two corresponding to increased Th/U (Fig. 1). Over the depth interval 3–8.6 μm, a weighted mean age [quoted at 2 standard error (S.E.)] of 3,876.2 ± 8.3 is indicated with an MSWD of three indicative of excess scatter likely due to an age gradient. From 8.8–17.2 μm and 17.4–25.7 μm, the weighted mean ages of 3,968.1 ± 5.0 (MSWD = 2.2) and 3,988.8 ± 5.1 Ma (MSWD = 1.8), respectively, show progressively less variance with the latter close to the expected range at 95% confidence (62). Some scatter is anticipated because temperatures across the profile climb above 850 °C and, thus, some Pb mobility via diffusion is expected. Excess variance could result from protracted growth over million year timescales or potentially be due to Pb loss from a rapidly crystallized overgrowth during subsequent residence at high temperature. We have evaluated several endmember scenarios using simple diffusion calculations to assess consistency with observation.

Scenario 1. The profile is due to continuous growth from 3,989 to 3,876 Ma at temperatures between 750 °C and 870 °C. The length scale for Pb diffusion in zircon (63) for heating at 870 °C for 110 million years is approximately 5 μm. This, however, is a lower bound as the possibility remains that rutile activity was subunity. For an $a_{TiO_2} \approx 0.5$ (25), we would need to add 80 °C to the calculated Ti-in-zircon temperature to correct for this effect. At *ca.* 930 °C, the calculated characteristic length scale is 36 μm—greater than the length of the depth profile. Thus, we can reasonably rule out scenario 1.

Scenario 2. The three cycles in [U] reflect growth during three discrete thermal episodes at *ca.* 3,876, 3,968, and 3,989 Ma between which temperature dropped below that of Pb closure. Assuming each event lasted no longer than the duration equivalent to 2 S.E. of the weighted mean age, the characteristic diffusion length scales for the average apparent temperature are 1.6, 0.5, and 0.1 μm, respectively. Even assuming $a_{TiO_2} \approx 0.5$ (i.e., adding 80 °C), the exchange length scales are still only 11, 5, and 1 μm and, thus, are broadly consistent with retaining apparent isochronous relationships within each [U] cycle.

Scenario 3. The two [U] cycles in which Th/U increases from 3,968 to 3,989 Ma reflect a single, protracted event with an average temperature of 790 °C. The characteristic calculated diffusion length scale of approximately 0.4 μm would be insufficient to significantly equilibrate across the nearly 20 μm-long-profile. This would also be true for the case where temperature was 80 °C higher (i.e., $\bar{x} = 4$ μm). Thus we can reasonably rule out scenario 1 but leave open the possibility that the profile contains two or three separate and relatively short duration thermal episodes.

The observed temperature interval (i.e., 750–870 °C) may be geologically meaningful as it corresponds to the transition from amphibolite to granulite facies during which breakdown of modal phases (64, 65) releases Zr that can nucleate new zircon and produce overgrowths on preexisting grains. The anticorrelation between Ti and U suggests that the pore fluid from which the zircon overgrowth grew was becoming progressively depleted in U as epitaxial growth continued under prograde conditions. The broadly held explanation for a rapid decrease in zircon Th/U is exposure of the pore fluid to an oxygenating environment resulting in uranium taking the +6 form that is highly soluble in aqueous solutions and potentially transportable relative to Th^{+4}. However, growth occurred more than 1.5 Ga prior to an oxygenating atmosphere (66). Other possible causes of decreasing [U] are growth of a coexisting U-rich phase that excludes Th, such as uraninite. Zircon growth, by contrast, would also draw down [Th], which is not apparent in the profile.

Conclusions

We have examined overgrowths on zircon cores predating the LHB to search for a signature of this hypothesized event for which no unambiguous terrestrial evidence has yet been documented. Specifically, we assessed the feasibility of combining ion-microprobe U-Th-Pb dating with Ti-in-zircon thermometry to reveal the temperature conditions under which these overgrowths formed. Whereas this coupled method can be used in spot mode, the depth profiling approach potentially provides continuous formation ages and temperatures with *ca.* 100 nm spatial resolution.

The slow rate of Pb transport under crustal conditions limits the likelihood that observed LHB-era U-Pb age gradients result from diffusion. Typically, the depth profile analyses show increasing U-Pb concordance from rim to core with the $^{207}Pb/^{206}Pb$ ages best characterizing the time of zircon growth. Depth-profiled zircons often exhibit high, near-surface concentrations of U, Th, and Ti—generally due to contamination—as well as near surface Pb*-loss.

Collectively, data from seven of the eight grains Ti-U-Th-Pb depth profiled yield $^{207}Pb/^{206}Pb$ ages >3,940 Ma with associated temperatures ranging from approximately 630–780 °C, in broad agreement with previous studies of terrestrial Hadean zircons providing documented temperatures ranging from 600–780 °C. Four of the eight Hadean zircons in this study preserve domains that yield ages between approximately 3,850 Ma and 3,950 Ma (i.e., *ca.* LHB-era) with temperatures ranging between approximately 840 °C and 875 °C, which are consistent with impact temperature spectra reaching temperatures to 900 °C. We recognize a bimodal temperature distribution with higher crystallization

temperatures seen in LHB-era growth zones and lower temperatures for older zircon domains. We suggest that the high LHB-era crystallization temperatures of these detrital zircons could, at least in part, reflect impact-related heating. Thus, high LHB-era temperature distribution could represent, to our knowledge, the first plausible terrestrial evidence of a thermal signature of the LHB.

1. Tera F, Papanastassiou DA, Wasserburg GJ (1974) Isotopic evidence for a terminal lunar cataclysm. *Earth Planet Sci Lett* 22:1–21.
2. Morbidelli A, Petit JM, Gladman B, Chambers J (2000) A plausible cause of the Late Heavy Bombardment. *Meteorit Planet Sci* 36:371–380.
3. Ryder G, Koeberl C, Mojzsis S (2000) *Origin of the Earth and Moon* (University Press Tucson, Tucson, AZ), pp 475–492.
4. Levison HF, et al. (2001) Could the lunar Late Heavy Bombardment have been triggered by the formation of Uranus and Neptune? *Icarus* 151:286–306.
5. Gomes R, Levison HF, Tsiganis K, Morbidelli A (2005) Origin of the cataclysmic late heavy bombardment period of the terrestrial planets. *Nature* 435:466–469.
6. Morbidelli A, Levison HF, Tsiganis K, Gomes R (2005) Chaotic capture of Jupiter's Trojan asteroids in the early Solar System. *Nature* 435:462–465.
7. Tsiganis K, Gomes R, Morbidelli A, Levison HF (2005) Origin of the orbital architecture of the giant planets of the solar system. *Nature* 435:459–461.
8. Turner G (1977) Potassium argon chronology of the moon. *Phys Chem Earth* 10:145–195.
9. Maurer P, et al. (1978) Pre-Imbrian craters and basins: Ages, compositions and excavation depths of Apollo 16 breccias. *Geochim Cosmochim Acta* 42:1687–1720.
10. McDougall I, Harrison TM (1999) *Geochronology and Thermochronology by the 40Ar/39Ar Method* (Oxford University Press, Oxford, NY), pp 233–234.
11. Baldwin RB (1974) Was there a terminal lunar cataclysm $3.9 - 4.0 \times 10^9$ years ago? *Icarus* 23:157–166.
12. Hartmann WK (1975) Lunar cataclysm: A misconception? *Icarus* 24:181–187.
13. Hartmann WK, Ryder G, Dones L, Grinspoon D (2000) *Origin of the Earth and the Moon*, eds R Canup and K Righter (University of Arizona Press, Tucson AZ), pp 805–826.
14. Warren PH (2004) *Treatise on Geochemistry*, eds HD Holland and KK Turekian (Elsevier, Amsterdam), pp 559–599.
15. Willbold M, Elliott T, Moorbath S (2011) The tungsten isotopic composition of the Earth's mantle before the terminal bombardment. *Nature* 477:195–198.
16. Trail D, Mojzsis SJ, Harrison TM (2007) Thermal events documented in Hadean zircons by ion microprobe depth profiles. *Geochim Cosmochim Acta* 71:4044–4065.
17. Condie KC (1984) Archean geotherms and supracrustal assemblages. *Tectonophysics* 105:29–41.
18. Davis DW, Williams IS, Krogh TE (2003) Historical development of zircon geochronology. *Rev Mineral Geochem* 53:145–181.
19. Finch RJ, Hanchar JM (2003) Structure and chemistry of zircon and zircon-group minerals. *Rev Mineral Geochem* 53:1–25.
20. Hoskin PW, Schaltegger U (2003) The composition of zircon and igneous and metamorphic petrogenesis. *Rev Mineral Geochem* 53:27–62.
21. Hanchar JM, Watson EB (2003) Zircon saturation thermometry. *Rev Mineral Geochem* 53:89–112.
22. Parrish RR, Noble SR (2003) Zircon U-Th-Pb geochronology by isotope dilution-thermal ionization mass spectrometry (ID-TIMS). *Rev Mineral Geochem* 53:183–213.
23. Ireland TR, Williams IS (2003) Considerations in zircon geochronology by SIMS. *Rev Mineral Geochem* 53:215–241.
24. Ireland TR, Williams IS (2003) Considerations in zircon geochronology by SIMS. *Rev Mineral Geochem* 53:215–241.
25. Watson EB, Harrison TM (2005) Zircon thermometer reveals minimum melting conditions on earliest Earth. *Science* 308:841–844.
26. Ferry J, Watson E (2007) New thermodynamic models and revised calibrations for the Ti-in-zircon and Zr-in-rutile thermometers. *Contrib Mineral Petrol* 154:429–437.
27. Mojzsis SJ, Harrison TM (2002) Establishment of a 3.83-Ga magmatic age for the Akilia tonalite (southern West Greenland). *Earth Planet Sci Lett* 202:563–576.
28. Abramov O, Mojzsis SJ (2009) Microbial habitability of the Hadean Earth during the late heavy bombardment. *Nature* 459:419–422.
29. Iizuka T, Horie K, Komiya T, Maruyama S, Hirata T (2006) 4.2 Ga zircon xenocryst in an Acasta Gneiss from northwestern Canada: Evidence for early continental crust. *Geology* 34:245–248.
30. Mojzsis SJ, Harrison TM (2000) Vestiges of a beginning: Clues to the emergent biosphere recorded in the oldest terrestrial sediments. *GSA Today* 10:1–6.
31. Froude DO, Ireland TR, Kinny PD, Williams IS, Compston W (1983) Ion microprobe identification of 4,100–4,200 Myr-old terrestrial zircons. *Nature* 304:616–618.
32. Williams IR, Myers JS (1987) Archaean geology of the mount Narryer region Western Australia. *Geol Surv West Aust* 22:1–32.
33. Kinny PD, Wijbrans JR, Froude DO, Williams IS, Compston W (1990) Age constraints on the geological evolution of the Narryer gneiss complex, Western Australia. *Aust J Earth Sci* 37:51–69.
34. Nutman AP, Kinny PD, Compston W, Williams IS (1991) SHRIMP U–Pb zircon geochronology of the Narryer gneiss complex, Western Australia. *Precambrian Res* 52:275–300.
35. Harrison TM (2009) The Hadean crust: Evidence from >4 Ga Zircons. *Annu Rev Earth Planet Sci* 37:479–505.
36. Compston W, Pidgeon RT (1986) Jack Hills, evidence of more very old detrital zircons in Western Australia. *Nature* 321:766–769.
37. Spaggiari CV, Pidgeon RT, Wilde SA (2007) The Jack Hills greenstone belt, Western Australia Part 2: Lithological relationships and implications for the deposition of ≥4.0 Ga detrital zircons. *Precambrian Res* 155:261–286.
38. Amelin YV (1998) Geochronology of the Jack Hills detrital zircons by precise U-Pb isotope dilution analysis of crustal fragments. *Chem Geol* 146:25–38.
39. Holden P, et al. (2009) Mass-spectrometric mining of Hadean zircons by automated SHRIMP multicollector and single-collector U/Pb zircon age dating: The first 100,000 grains. *Int J Mass Spectrom* 286:53–63.
40. Myers JS, et al. (1990) *Third International Archean Symposium, Perth, Excursion Guidebook*, eds SE Ho, JE Glover, JS Myers, and JR Muhling (University of Western Australia, Perth, WA), 21, pp 61–95.
41. Cavosie AJ, Wilde SA, Liu D, Weiblen PW, Valley JW (2004) Internal zoning and U-Th-Pb chemistry of Jack Hills detrital zircons: A mineral record of early Archean to Mesoproterozoic (4348–1576 Ma) magmatism. *Precambrian Res* 135:251–279.
42. Maas R, Kinny PD, Williams I, Froude DO, Compston W (1992) The Earth's oldest known crust: A geochronological and geochemical study of 3900–4200 Ma old detrital zircons from Mt. Narryer and Jack Hills, Western Australia.. *Geochim Cosmochim Acta* 56:1281–1300.
43. Peck WH, Valley JW, Wilde SA, Graham CM (2001) Oxygen isotope ratios and rare earth elements in 3.3–4.4 Ga zircons: Ion microprobe evidence for high δ18O continental crust and oceans in the early archean. *Geochim Cosmochim Acta* 65:4215–4229.
44. Harrison TM, et al. (2005) Heterogeneous Hadean hafnium: Evidence of continental crust by 4.4–4.5 Ga. *Science* 310:1947–1950.
45. Paces JB, Miller JD (1993) Precise U-Pb ages of Duluth Complex and related mafic intrusions, northeastern Minnesota: Geochronological insights into physical, petrogenetic, and paleomagnetic and tectomagnetic processes associated with the 1.1 Ga mid-continent rift system. *J Geophys Res* 98:13997–14013.
46. Schmitz MD, Bowring SA, Ireland TR (2003) Evaluation of Duluth Complex anorthositic series (AS3) zircon as a U-Pb geochronological standard: New high-precision isotope dilution thermal ionization mass spectrometry results. *Geochim Cosmochim Acta* 67:3665–3672.
47. Wiedenbeck M, et al. (1995) Three natural zircon standards for U-Th-Pb, Lu-Hf, trace element, and REE analyses. *Geostand Geoanal Res* 19:1–23.
48. Breeding CM, Ague JJ, Grove M, Rupke AL (2004) Isotopic and chemical alteration of zircon by metamorphic fluids: U–Pb age depth-profiling of zircon crystals from Barrow's garnet zone, northeast Scotland. *Am Mineral* 89:1067–1077.
49. Black LP, et al. (2004) Improved $^{206}Pb/^{238}U$ microprobe geochronology by the monitoring of a trace-element-related matrix effect; SHRIMP, ID-TIMS, ELA-ICP-MS, and oxygen isotope documentation for a series of zircon standards. *Chem Geol* 205:115–140.
50. Aikman AB (2007) *Tectonics of the Eastern Tethyan Himalaya* (Australian National University, Canberra, Australia), pp 1–327.
51. Grove M, Harrison TM (1999) Monazite Th-Pb age depth profiling. *Geology* 27:487–490.
52. Watson EB, Wark DA, Thomas JB (2006) Crystallization thermometers for zircon and rutile. *Contrib Mineral Petrol* 151:413–433.
53. Stacey JS, Kramers JD (1975) Approximation of terrestrial lead isotope evolution by a two-stage model. *Earth Planet Sci Lett* 26:207–221.
54. Bell EA, Harrison TM, McCulloch MT, Young ED (2011) Early Archean crustal evolution of the Jack Hills zircon source terrane inferred from Lu-Hf, $^{207}Pb/^{206}Pb$, and δ18O systematics of Jack Hills zircons. *Geochim Cosmochim Acta* 75:4816–4829.
55. Harrison TM, Schmitt AK (2007) High sensitivity mapping of Ti distributions in Hadean zircons. *Earth Planet Sci Lett* 261:9–19.
56. Wielicki MM, Harrison TM, Schmitt AK (2012) Geochemical signatures and magmatic stability of terrestrial impact produced zircon. *Earth Planet Sci Lett* 321:20–31.
57. Cherniak DJ, Watson EB (2007) Ti diffusion in zircon. *Chem Geol* 242:473–483.
58. Shannon RD (1976) Revised effective ionic radii and systematic studies of interatomic distances in halides and chalcogenides. *Acta Crystallographica A* 32:751–767.
59. Abbott SS (2011) *A search for terrestrial evidence for the Late Heavy Bombardment in Ti-U-Th-Pb depth profiles of Hadean zircons* (University of California, Los Angeles, Los Angeles, CA), pp 1–156.
60. Harrison TM, Aleinikoff JN, Compston W (1997) Observations and controls on the occurrence of inherited zircons in Concord-type granitoids, New Hampshire. *Geochim Cosmochim Acta* 51:2549–2558.
61. Williams IS, Compston W, Black LP, Ireland TR, Foster JJ (1984) Unsupported radiogenic Pb in zircon: A cause of anomalously high Pb-Pb, U-Pb and Th-Pb ages. *Contrib Mineral Petrol* 88:322–327.
62. Wendt I, Carl C (1991) The statistical distribution of the mean square weighted deviation. *Chem Geol* 86:275–285.
63. Cherniak DJ, Watson EB (2001) Pb Diffusion in zircon. *Chem Geol* 172:5–24.
64. Degeling H, Eggins S, Ellis DJ (2001) Zr budgets for metamorphic reactions, and the formation of zircon from garnet breakdown. *Mineral Mag* 65:749–758.
65. Rubatto D, Williams IS, Buick IS (2001) Zircon and monazite response to prograde metamorphism in the Reynolds range, Central Australia. *Contrib Mineral Petrol* 140:458–468.
66. Farquhar J, Bao H, Thiemens M (2000) Atmospheric influence of Earth's earliest sulfur cycle. *Science* 289:756–758.